CHEMISTRY OF MATERIALS

pubs.acs.org/cm

Article

# Structural Inhomogeneities and Suppressed Magnetostructural Coupling in Mn-Substituted $GeCo_2O_4$

Shivani Sharma,* Pooja Jain, Benny Schundelmier, Chin-Wei Wang, Poonam Yadav, Adrienn Maria Szucs, Kaya Wei, Niranjan P. Lalla, and Theo Siegrist

Cite This: *Chem. Mater.* 2025, 37, 5995−6003

Read Online

ACCESS | Metrics & More | Article Recommendations

**ABSTRACT:** A comprehensive study of the $Ge_{1-x}Mn_xCo_2O_4$ (GMCO) system was conducted using neutron powder diffraction (NPD), X-ray diffraction (XRD), scanning electron microscopy, magnetometry, and heat capacity measurements. Comparative analysis with $GeCo_2O_4$ (GCO) highlights the influence of Mn substitution on crystal and magnetic structures at low temperatures. Surprisingly, phase separation is observed in GMCO with a targeted nominal composition with Ge/Mn close to 50:50. Scanning electron microscopy/energy-dispersive X-ray (SEM/EDX) analysis reveals pronounced compositional inhomogeneities, which are not evident in the XRD data. The GMCO sample predominantly consists of a Mn-rich primary phase with approximate stoichiometry $Mn_{0.74}Ge_{0.18}Co_2O_4$, along with a minor Ge-rich secondary phase of composition $Ge_{0.91}Mn_{0.18}Co_2O_4$. Although both GCO and GMCO crystallize in cubic symmetry at room temperature, a substantial difference in low-temperature structural properties has been observed. Magnetic and heat capacity data indicate ferrimagnetic ordering in $Mn_{0.74}Ge_{0.18}Co_2O_4$ near $T_c$ = 108 K, while $Ge_{0.91}Mn_{0.18}Co_2O_4$ exhibits antiferromagnetic order at $T_N$ = 22 K. Analysis of heat capacity data reveals that the estimated magnetic entropy amounts to only 56% of the theoretical value expected in GMCO. A collinear ferrimagnetic arrangement is observed in $Mn_{0.74}Ge_{0.18}Co_2O_4$ below the magnetic ordering temperature, characterized by antiparallel spins of Mn at the A site and Co at the B site along the c-direction. At 5 K, the refined magnetic moments are 2.31(3) $\mu_B$ for $Mn_A$ and 1.82(3) $\mu_B$ for $Co_B$ in the $Mn_{0.74}Ge_{0.18}Co_2O_4$ phase. The magnetic structure at 5 K in $Ge_{0.91}Mn_{0.18}Co_2O_4$ is identical to the antiferromagnetic structure of the parent compound $GeCo_2O_4$. The refined value of the $Co_B$ moment in this phase at 5 K is 2.53(3) $\mu_B$.

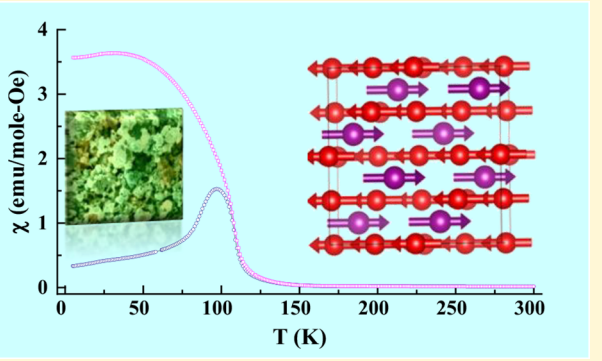




## INTRODUCTION

Over the past several decades, the exploration of frustration in magnetic systems has been a subject of intense interest, primarily driven by the captivating magnetic states, such as spin glass or spin liquid in strongly correlated electron systems.[1−10] One of the most studied origins of frustration in magnetic systems is the geometrical arrangement of the first nearest-neighbor antiferromagnetic (AFM) interactions in triangular (2D), tetrahedral (3D), pyrochlore, or Kagome lattices.[5,10−14] This work particularly focuses on geometrically frustrated systems, exemplified by Co-based cubic spinel structures ($ACo_2O_4$), where Co atoms are arranged in alternate triangular and Kagome lattices, stacked along the [111] direction as shown in Figure 1.[3,4,13,15−20] Due to the corner-sharing tetrahedra of B-site cations (see Figure 1a) forming the pyrochlore lattice, the cubic spinel exhibits geometrical frustration.[8,18,21−23]

Spinel oxides, known for their versatile structural frameworks and rich physical properties, are broadly categorized based on the distribution of cations among the tetrahedral (A) and octahedral (B) sites into two types: normal and inverse spinels. In a normal spinel structure, the A-site cations exclusively occupy the tetrahedral sites, while the B-site cations reside in the octahedral sites. Each formula unit consists of eight tetrahedral and four octahedral sites. A representative example of a normal spinel is $GeCo_2O_4$ (GCO), which has been extensively studied for its structural and magnetic characteristics.[19] In contrast, an inverse spinel structure features a more complex cation arrangement, where all A-site cations and half of the B-site cations occupy the octahedral sites and the remaining B-site cations are located on the tetrahedral sites. $MnCo_2O_4$ (MCO) is a prototypical inverse spinel, known for its distinct cation ordering and

Received: May 28, 2025
Revised: July 24, 2025
Accepted: July 25, 2025
Published: August 2, 2025

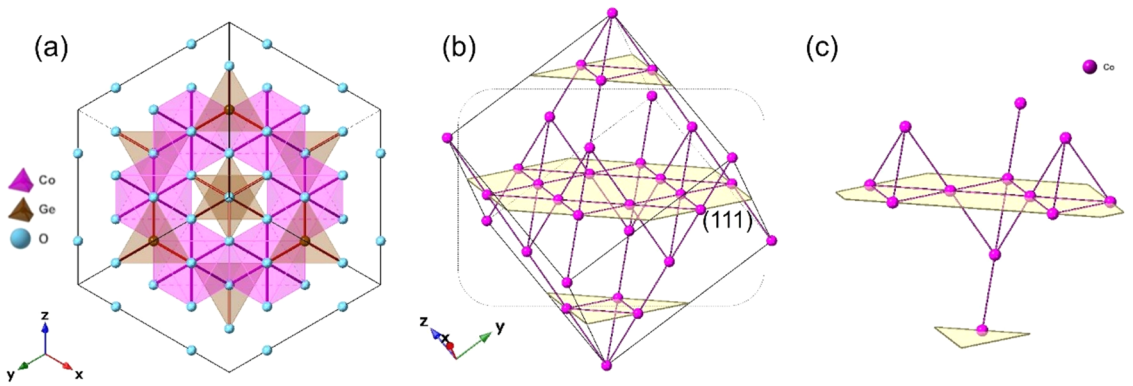


**Figure 1.** (a) Crystal structure of the spinel compound projected along the [111] direction, highlighting the network of corner-sharing $CoO_6$ (pink octahedra) and $GeO_4$ (brown tetrahedra) units within the cubic oxygen (blue spheres) framework. (b) Three-dimensional view of the Co sublattice emphasizing the pyrochlore network, with the (111) plane highlighted. (c) Zoomed-in view of the Kagome-triangular stacking motif in the Co sublattice along the [111] direction, illustrating the alternating arrangement of Kagome and triangular layers characteristic of geometrically frustrated systems.

related magnetic behavior.[24,25] Both GCO and MCO have attracted significant research attention due to their contrasting cation distributions and the resulting influence on their structural and magnetic properties, making them ideal systems for probing the interplay among lattice geometry, electronic configuration, and magnetism in spinel compounds.

GCO, in particular, has garnered significant attention due to its unique electronic and magnetic ground state, featuring octahedral $Co^{2+}$ ions. This state is characterized by a high-spin $3d^7$ configuration with $S = 3/2$, $L = 3$, yet is more accurately described as a Kramer's doublet with $J_{eff} = 1/2$. The presence of orbitally degenerate $t_{2g}^5$ states in the high-spin octahedral $Co^{2+}$ leads to substantial spin−orbit coupling, resulting in pronounced single-ion anisotropy, a distinctive trait for a 3d transition metal. Below its Néel temperature ($T_N \cong 21$ K), GCO undergoes AFM ordering with a characteristic wave vector $k = [1/2,1/2,1/2]$, accompanied by a structural phase transition from cubic to lower symmetry.[3,4,11−13,15,19,21,26] Neutron studies conducted by multiple research groups offer a cohesive understanding of the spin ordering in GCO.[3,12,21,26] In contrast, MCO has been studied for its remarkable magnetic properties and colossal magnetoresistance behavior.[24,25]

Given the intriguing physical and structural properties of spinel compounds like GCO and MCO, and the demonstrated sensitivity of these properties to compositional modifications, extensive efforts have been directed toward exploring A- and/or B-site-substituted spinels. Substitutions at either site (A or B) can profoundly alter the magnetic ground state, introduce new ordering phenomena, or even tune the $T_c$ (transition temperatures). For example, neutron powder diffraction (NPD) studies on $Co_2Ru_{1-x}Mn_xO_4$ have shown that progressive Ru substitution modifies the magnetic ground state, giving rise to two distinct transitions at 100 and 180 K.[25,27] Similarly, Bi substitution at the A site in MCO has been reported to significantly enhance the magnetic transition temperature up to 200 K.[28] Further, ferrimagnetic ordering was confirmed at 184 and 164 K in off-stoichiometric $Mn_{1.15}Co_{1.85}O_4$ and $Mn_{1.17}Co_{1.60}Cu_{0.23}O_4$ as well as as in $Ti_{0.6}Mn_{0.4}Co_2O_4$ and $Ti_{0.8}Mn_{0.2}Co_2O_4$ below 110.3 and 78.2 K,[29,30] confirming the versatility of magnetic interactions in substituted spinel systems. While prior studies have thoroughly examined the end members of such systems, the effect of targeted substitution—particularly of Mn at the Ge site in GCO—remains insufficiently understood. This substitution pathway is especially compelling as it offers the potential to bridge the contrasting behaviors of GCO (a normal spinel with pronounced spin−orbit coupling) and MCO (an inverse spinel with ferrimagnetic ordering and magnetoresistance). Despite its promise, only limited work exists on Mn-substituted $Ge_{1-x}Mn_xCo_2O_4$, with a recent report focusing on 20% Mn substitution based solely on bulk magnetization data, offering a limited understanding of the low-temperature magnetic and structural properties.[31] Therefore, a detailed investigation of Mn-substituted GCO—spanning structural, magnetic, and thermodynamic properties—is essential to uncover the evolution of crystal and magnetic structures and the role of spin−lattice coupling in this complex spinel system.

To address this gap, a comprehensive study of $GeCo_2O_4$ and $Ge_{1-x}Mn_xCo_2O_4$ (GMCO) has been performed using a combination of NPD, X-ray diffraction (XRD), scanning electron microscopy/energy-dispersive X-ray (SEM/EDX), magnetometry, and heat capacity techniques. The end compounds, GCO and MCO, crystallize in cubic and tetragonal structures at room temperature, respectively, with the structural distortion in MCO arising from the Jahn−Teller active $Mn^{3+}$ ions.[6,19,24] Consequently, Mn substitution in GCO is expected to induce changes in crystal symmetry and geometrical frustration, thereby influencing the nature and strength of magnetic exchange interactions. This study is focused on understanding the impact of Mn substitution on the crystallographic symmetry and magnetic ground state of GMCO, given the sensitivity of spinel systems to cationic substitution. Comparative analysis with parent compound GCO reveals that Mn substitution leads to distinct structural and magnetic properties, particularly at low temperatures. SEM/EDX analysis indicates clear phase separation, with a Mn-rich primary phase $Mn_{0.74}Ge_{0.18}Co_2O_4$ and Ge-rich minor phase $Ge_{0.91}Mn_{0.18}Co_2O_4$ in GMCO. Magnetic measurements show that $Mn_{0.74}Ge_{0.18}Co_2O_4$ undergoes ferrimagnetic ordering at 108 K, while $Ge_{0.91}Mn_{0.18}Co_2O_4$ retains AFM ordering near 22 K, consistent with the behavior of pure GCO. These findings highlight the pivotal role of cation substitution in modulating the interplay among spin, lattice, and orbital degrees of freedom in spinel oxides.


https://doi.org/10.1021/acs.chemmater.5c01331
Chem. Mater. 2025, 37, 5995−6003

## EXPERIMENTAL SECTION

Polycrystalline samples of GCO and GMCO with a targeted nominal Ge/Mn ratio of 50:50 were prepared via the solid-state reaction method.[4,15,18,21] The starting materials $GeO_2$ (99.99% purity), $MnO_2$ (99.99% purity), and $Co_2O_3$ (99.99% purity) were mixed in stoichiometric amounts. The resulting mixture was then calcined at 950 °C for 12 h and sintered at 950 °C for another 12 h. To verify the phase purity of the prepared compounds and to investigate the low-temperature structural phase transitions, powder X-ray diffraction (XRD) measurement was recorded as a function of temperature using Rigaku's diffractometer equipped with Cu-K$\alpha$ radiation. High-resolution imaging, backscattered electron X-ray (BEX), and energy-dispersive X-ray (EDX) analyses were performed using a Tescan MIRA 4 field emission scanning electron microscope (FE-SEM) equipped with an Oxford Instruments Unity BEX Imaging Detector and Ultim Max 170 $mm^2$ EDX detectors. BEX imaging was utilized to examine the raw powder sample, providing both topographical and compositional contrast, enabling the observation of chemical variations. For EDX analysis, the sample was epoxy-mounted and polished. For EDX analysis, a beam current of 1 nA was used at 20 kV. BEX imaging was conducted at 20 kV with a beam current of 3 nA, with an image scan and X-ray scan size of 1024, a dwell time of 400 $\mu$s, and an overall frame time of 419.4 s. Data processing and analysis were performed using Oxford Instruments Nano-Analysis AZtec software. DC magnetic susceptibility measurements were done using a superconducting quantum interference device (SQUID) as a function of temperature and field, and the heat capacity was measured using a physical property measurement system. Powder neutron diffraction measurements on GMCO were carried out at ECHIDNA and WOMBAT beamlines at the OPAL facility, ANSTO, Australia. The room-temperature data from the ECHIDNA beamline with neutron wavelength of 1.62 Å was used to estimate the chemical composition of the Mn-substituted compound. Temperature-dependent data from WOMBAT beamline with neutron wavelength of 2.41 Å was used for magnetic structure analysis as a function of temperature for a broad range of temperatures ranging from 5 to 120 K. Fullprof suit and JANA were used for magnetic structure refinement.[32]

## RESULT AND DISCUSSION

**Room-Temperature Structural Properties.** Figure 2a,b shows the Rietveld refined XRD patterns of $GeCo_2O_4$ and GMCO recorded at room temperature. For both compositions, all of the observed peaks are very well fitted with a single cubic spinel structure with space group $Fd\bar{3}m$, consistent with the reported crystal structures of GCO and $Ge_{0.8}Mn_{0.2}Co_2O_4$.[31] In the case of GMCO, initially, the refinement was performed assuming a random distribution of $Ge^{4+}$ and $Mn^{4+}$ and constraining the ratio of Ge/Mn to 50:50 at the tetrahedral site 8*b*. $Co^{2+}$ is situated at the octahedral site 16*c* and $O^{2-}$ at site 32*e*. A reasonably good refinement was achieved this way. Further, to get more accurate cationic distribution using XRD, the Ge and Mn occupancies were refined by constraining their combined occupation to 1. The resultant refinement (shown in Figure 2b) gives a slightly better fit to the data than a fixed occupancy (Ge/Mn = 50:50) model. The goodness-of-fit parameter also decreases from 1.29 to 1.25. The refined occupancies obtained through the XRD data suggest a Ge/Mn ratio of 20:80 in the sample, which is very different from the expected values (50:50). This is further confirmed using EDX, as discussed in the subsequent section. The refined lattice parameters for GCO and GMCO are $a$ = 8.3095(6) and 8.3085(6) Å, respectively. The inset in each panel of Figure 2 enlarges the (008) reflection exhibiting Cu $K_{\alpha1}$ and $K_{\alpha2}$ splitting. Further, no extra peak at the lower scattering angle was observed, which indicates that Ge and Mn are randomly distributed at the 8*b* site. In the XRD data, no trace of the secondary phase was evident, and this will be further discussed in the subsequent sections.

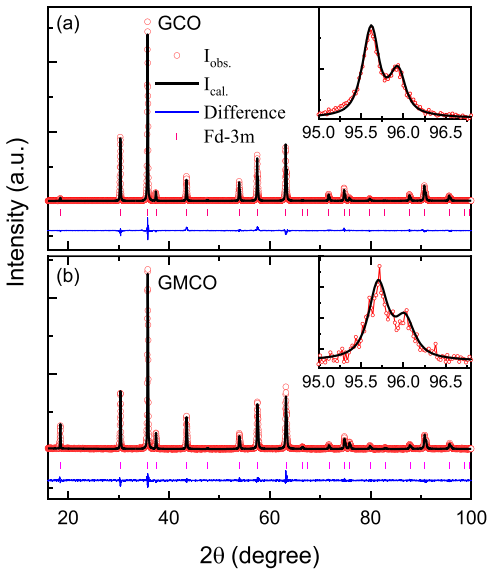


**Figure 2.** Rietveld refined room-temperature XRD patterns of (a) $GeCo_2O_4$ and (b) $Ge_{0.5}Mn_{0.5}Co_2O_4$using the $Fd\bar{3}m$ spinel structure. The inset in each panel zooms in on the (008) reflection with Cu $K_{\alpha1}$ and $K_{\alpha2}$ splitting.

To better visualize the cation distribution and compositional inhomogeneity, high-resolution imaging, backscattered electron X-ray (BEX), and energy-dispersive X-ray (EDX) analyses have been performed on GMCO. The BEX layered and SE images given in Figure 3a,b provide an overview of the sample, showing grain size distribution and compositional variations across different regions, with grain sizes generally below 5 $\mu$m and noticeable material clustering. The EDX spectra on the powder sample over a broad area gives the stoichiometric ratio close to $Ge_{0.5}Mn_{0.5}Co_2O_4$ but the detailed EDX on epoxy-mounted samples shows striking compositional inhomogeneities, which are crucial to understand the magnetostructural properties in this compound.

SEM-EDX analysis of the epoxy-mounted sample shows two distinct compositional phases, marked as regions A and B in Figure 4. The BEX image shows a clear color contrast between the two phases: green (region A) and yellow (region B). Region A is Mn-rich, while region B is Ge-rich, indicating the presence of two distinct compositional phases in the sample. Both regions exhibit compositions close to the $AB_2O_2$ stoichiometry, with Ge/Mn at the A site and Co at the B site; however, they differ in the A-site occupancy. The major phase (region A) exhibits a composition approximating $Mn_{0.74}Ge_{0.18}Co_2O_4$ (Figure 4, Spectrum A), whereas the Ge-rich secondary phase (region B) is closer to $Ge_{0.91}Mn_{0.18}Co_2O_4$ (Figure 4, Spectrum B). These results show that despite XRD indicating a uniform stoichiometry and single-phase nature of the sample, microscopic analysis reveals significant local compositional inhomogeneities. The Ge/Mn ratio in the main phase $Mn_{0.74}Ge_{0.18}Co_2O_4$ is close to 20:80 (in percentage), which was also realized through XRD analysis. However, due to similar lattice parameters and similar cations in the secondary phase (as compared to the main phase), standard laboratory XRD generally lacks the resolution to distinguish them, highlighting the need for complementary techniques such as EDX and NPD.


https://doi.org/10.1021/acs.chemmater.5c01331
Chem. Mater. 2025, 37, 5995−6003

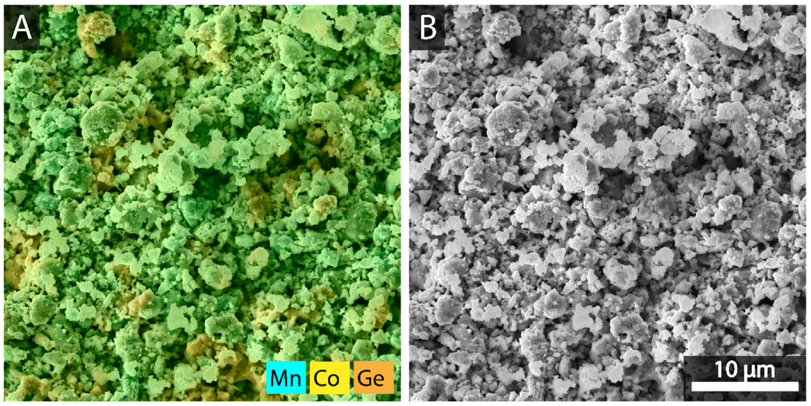


**Figure 3.** (A) SEM-BEX layered and (B) SE image of the Mn−Ge−Co sample, illustrating the overall microstructure, grain size, and chemical composition variations, with locations marked for Spectrum A and Spectrum B, where EDX spectra were collected. The spectra display variations in Ge/Mn ratios, corresponding to two distinguishable compositions. The measured values are given in the inset.

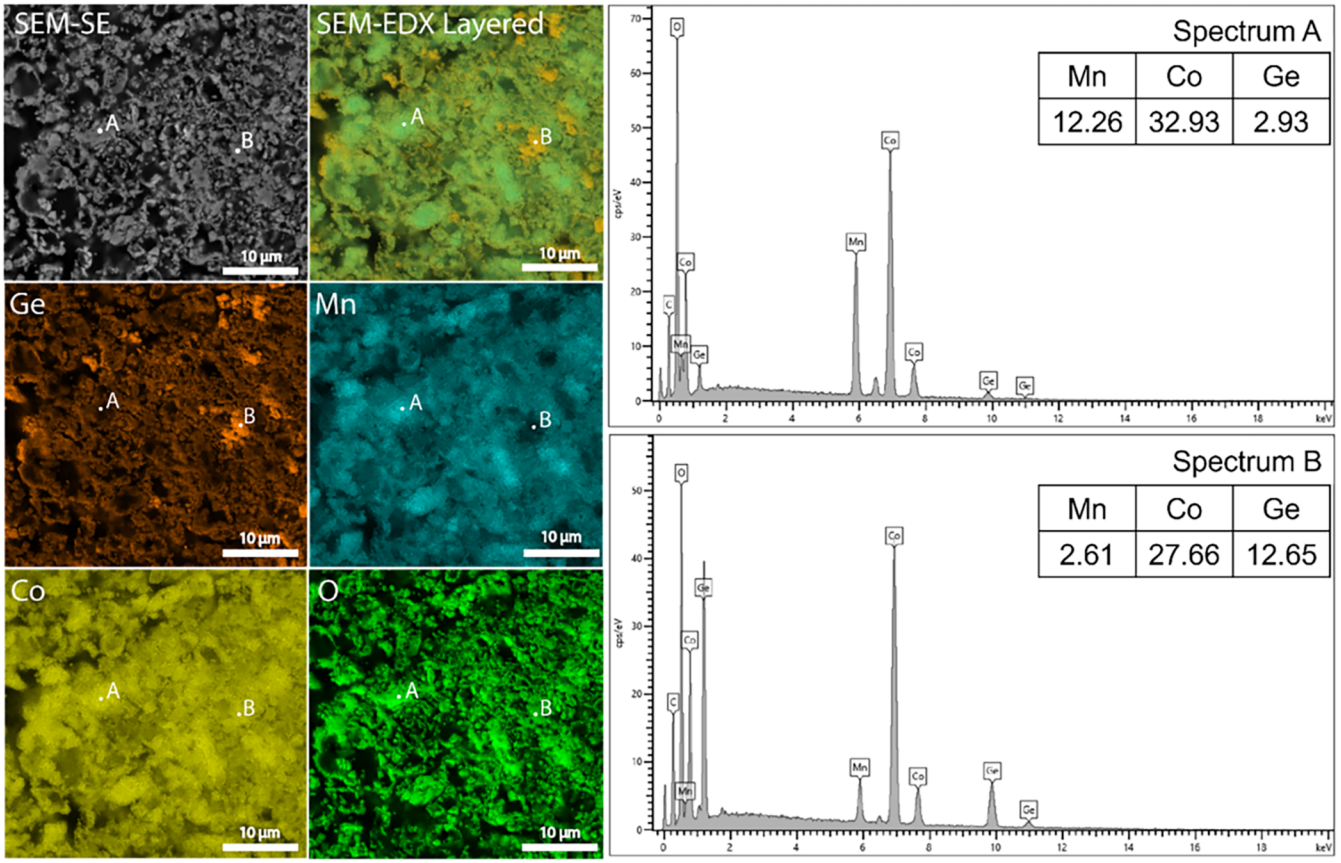


**Figure 4.** SEM-EDX analysis results on the epoxy-mounted sample showing secondary electron (SE) imaging, EDX layered mapping, and elemental composition maps, with locations marked for A and B, where EDX spectra were collected. The spectra display variations in Ge/Mn ratios, corresponding to two distinguishable compositions.

Due to the substantial difference in the neutron scattering lengths for Mn (−3.73 fm) and Ge (8.185 fm), neutron diffraction experiments provide an advantage over XRD for confirming the compositional inhomogeneities in GMCO. The NPD pattern from the ECHIDNA beamline was analyzed to check for the possible phase inhomogeneity in the as-prepared samples. The initial model, which assumed both Ge(50%) and Mn(50%) at the A site, failed to capture the full intensity of several reflections. Even after several iterations and checking all of the possibilities of cation distribution at the A and B sites, this model could not capture the full intensity of some of the reflections, as shown in Figure 5a. To account for the full intensities of these reflections, an additional phase was added using the insight gained from SEM/EDX analysis. The corresponding refined pattern is presented in Figure 5b. With the two-phase model, due to the very similar cation distribution in these phases, the refinement was nontrivial. To ensure stability in the refinement, the chemical compositions of the two phases were fixed as $Mn_{0.74}Ge_{0.18}Co_2O_4$ (main phase) and $Ge_{0.91}Mn_{0.19}Co_2O_4$, based on EDX data. The value of $\chi^2$


https://doi.org/10.1021/acs.chemmater.5c01331
Chem. Mater. 2025, 37, 5995−6003

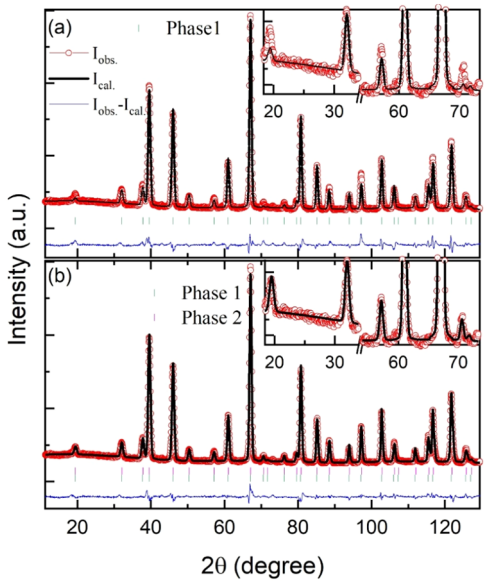


**Figure 5.** Rietveld refinement of room-temperature neutron powder diffraction patterns for $Ge_{1-x}Mn_xCo_2O_4$ using a (a) single-phase model with $x = 0.5$ and (b) two-phase model with $Mn_{0.74}Ge_{0.18}Co_2O_4$ as the primary phase and $Ge_{0.91}Mn_{0.19}Co_2O_4$ as the minor phase. The insets highlight the $2\theta$ range of 20−70°, where noticeable discrepancies in peak intensities are observed for the single-phase model, while the two-phase refinement provides significantly improved agreement with the experimental data, indicating phase coexistence in the sample.

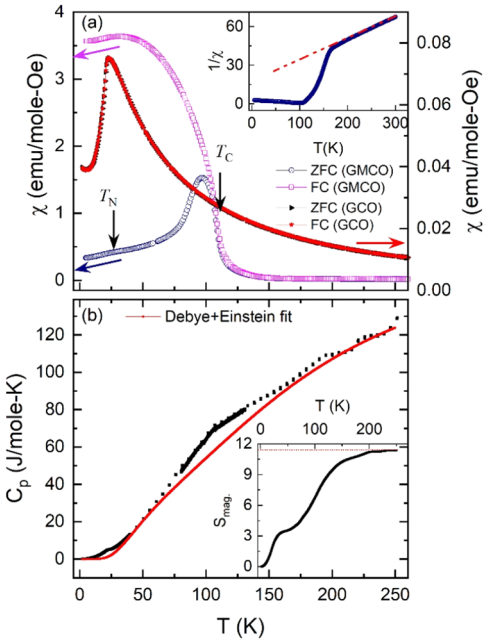


**Figure 6.** Temperature-dependent (a) DC magnetic susceptibilities of GCO and GMCO, measured with 500 Oe and (b) heat capacity of GMCO. Inset in panel (a) shows the Curie−Weiss (CW) fit (red line) to the inverse susceptibility data for GMCO. Inset in panel (b) displays the magnetic entropy change associated with the two magnetic transitions. The red line in panel (b) represents the lattice contribution modeled using a combination of Debye and Einstein terms.

was reduced from 7.59 to 3.75, while the value of $R_{wp}$ was reduced from 14.6 to 9.86 compared to the fit given in Figure 5a. The refined lattice parameter for the primary phase $Mn_{0.74}Ge_{0.18}Co_2O_4$ is $a = 8.29642(7)$ Å, and for the secondary phase $Ge_{0.91}Mn_{0.19}Co_2O_4$, $a = 8.30751(8)$ Å, slightly larger by about 0.13%. The estimated phase fraction of the secondary $Ge_{0.91}Mn_{0.19}Co_2O_4$ is 6.3(4)% and it is kept fixed for the refinement of the low-temperature NPD data for the subsequent sections. In the crystal structure of $Mn_{0.74}Ge_{0.18}Co_2O_4$, the Mn/Ge atoms occupy the Wyckoff position 8*b* at the coordinates (1/8, 1/8, 1/8), Co at 16*c* (1/2, 1/2, 1/2) and the O atoms reside at the 32*e* site with fractional coordinates (*z*, *z*, *z*) where $z = 0.2533(1)$. The isotropic mean square displacement parameter *B* values for Ge/Mn, Co, and O are 0.91(5), 0.65(5), and 1.10(1) $Å^2$, respectively. Due to the small amount of the secondary phase, it was not possible to refine the individual atomic displacement parameters in this minor phase and an overall *B* factor was instead refined.

**Physical Properties.** To investigate the effect of Mn substitution on the magnetic properties, the magnetic susceptibility of GMCO is compared to GCO. Figure 6a shows the magnetic susceptibility $\chi(T)$ curves of both samples measured between 2 and 300 K under zero-field-cooled (ZFC) and field-cooled (FC) conditions in an applied field of 500 Oe. The $\chi(T)$ of pristine GCO reveals a single AFM transition at $T_N = 22$ K, consistent with the literature values.[3,18,33] For GMCO, ZFC $\chi(T)$ rises sharply below 120 K, showing a peak near 95 K with a clear bifurcation between ZFC and FC below it. The transition temperature, estimated from the first derivative, is $T_c = 108$ K and is associated with the ferrimagnetic (FiM) ordering of A- and B-site spins in the Mn-rich main phase, as confirmed by neutron diffraction data. At lower temperatures, a subtle kink appears around $T_N$ = 22 K, more prominently seen in the heat capacity data (Figure 6b). This second transition is attributed to the AFM ordering of Co spins in the Ge-rich phase. The isothermal magnetization curves are typical for a ferrimagnetic lattice with a large anisotropy below $T_c$. In $MnCo_2O_4$, the FiM order takes place below 184 K, whereas the FiM transition temperature decreases to 77 K for $Ge_{0.8}Mn_{0.2}Co_2O_4$.[24,31] In the present case, with $Mn_{0.74}Ge_{0.18}Co_2O_4$ as the main phase, the transition temperature is in line with other members of this family. The inverse magnetic susceptibility in the inset of Figure 6a exhibits deviance from the Curie−Weiss (CW) behavior below 200 K, indicating that the magnetic interactions start far above $T_c$. Moreover, the Curie constant of 6.04 corresponds to an effective paramagnetic moment of 6.95(±0.03) $\mu_B$/f.u. The value of the Weiss temperature ($\theta_C$) is −107.4 K. Considering the cation distribution as $Mn_{0.74}Ge_{0.18}Co_2O_4$, the spin only value of $\mu_{eff}$ is 6.40 for high-spin states and 4.12 $\mu_B$ for low spin states of $Co^{2+}$. In the absence of JT distortions (and associated structural transition), the observed value of $\mu_{eff}$ is consistent with high-spin state of $Co^{2+}$ ions.

The heat capacity and magnetic entropy ($S_{mag}$) of GMCO are presented in Figure 6b. A broad transition with a peak center at 108 K ($T_c$) is observed in the data, associated with the FiM order of Mn and Co ions in $Mn_{0.74}Ge_{0.18}Co_2O_4$. An additional sharp peak at 22 K is also evident, linked with the AFM ordering of Co ions in the $Ge_{0.91}Mn_{0.18}Co_2O_4$ phase. The broad nature of the high-temperature transition is attributed to small variations of the Ge/Mn ratio (2−3%) across different regions of the $Mn_{0.74}Ge_{0.18}Co_2O_4$ sample, as confirmed through SEM/EDX analysis. A combination of Debye and Einstein models is used to evaluate the lattice specific heat.[34] The estimated value for the magnetic entropy is 11.26 J/mol


https://doi.org/10.1021/acs.chemmater.5c01331
Chem. Mater. 2025, 37, 5995−6003

K. Assuming $Mn^{4+}$ at the A site and $Co^{2+}$ at the B site, this value is only 56% of the expected value for $Mn_{0.74}Ge_{0.18}Co_2O_4$, similar to the reported values for other members of this family. An alternative method based on harmonic lattice approximation was used by Lashley et al.[4] to estimate the magnetic entropy for GCO and $GeNi_2O_4$, which yields almost identical results. The reported values of magnetic entropy were 58.3 and 56.5% in the case of GCO and $GeNi_2O_4$, and the missing entropy was suspected to be originating from substantial magnetic correlations well above the magnetic ordering.[4]

**Low-Temperature Structural Properties.** To investigate the possible structural changes associated with AFM ordering, XRD patterns in the selected $2\theta$ range were recorded for both GCO and GMCO, while the samples were cooled from 25 to 12 K. Figure 7a,b shows the temperature evolution of the (0 0 8) reflection. Clear splitting of the (0 0 8) reflection (both $K_{\alpha1}$ and $K_{\alpha2}$) at the cubic to tetragonal ($I4_1/amd$) transition in GCO, associated with the magnetic order, is observed. Regarding the splitting in GCO, it can be seen starting from $T_N$ (= 21 K). Earlier, Barton et al.[19] argued that the structural transition in GCO is decoupled from the magnetic transition based on powder data. However, in the present case, it occurs at the same temperature, indicating strong coupling between the structural and magnetic orders. Similar distortion at the Néel temperature in CoO has been under debate. While some reports indicate spin−orbit coupled magnetostriction[3,35] arises due to degenerate $t_{2g}$ states in octahedral $Co^{2+}$, others suggest JT ordering.[36,37] Interestingly, no such peak splitting or peak broadening effect was observed for GMCO, indicating that it remains cubic down to 12 K. Furthermore, the full width at half-maximum (FWHM) of (0 0 8) reflection remains almost invariant upon cooling. The estimated values of FWHM at 160 and 12 K are 0.322(1) and 0.319(9)°, respectively, confirming the absence of structural phase transition in GMCO within the resolution of the measurement. The origin of structural distortion in these systems with degenerate $t_{2g}$ states is usually the result of coupled effects of spin, orbital, and lattice degrees of freedom. Due to the complex cation distribution in the GMCO and several possible factors contributing to the distortions in these compounds, it is nontrivial to pinpoint a specific cause for the absence of a structural phase transition. Moreover, these distortions can be suppressed or decoupled from the magnetic ordering, resulting in the onset of AFM ordering without any accompanying structural transition.[36] Suppression of structural transition in the presence of minute Mn at the A site was also evident for the other members of this family.[29]

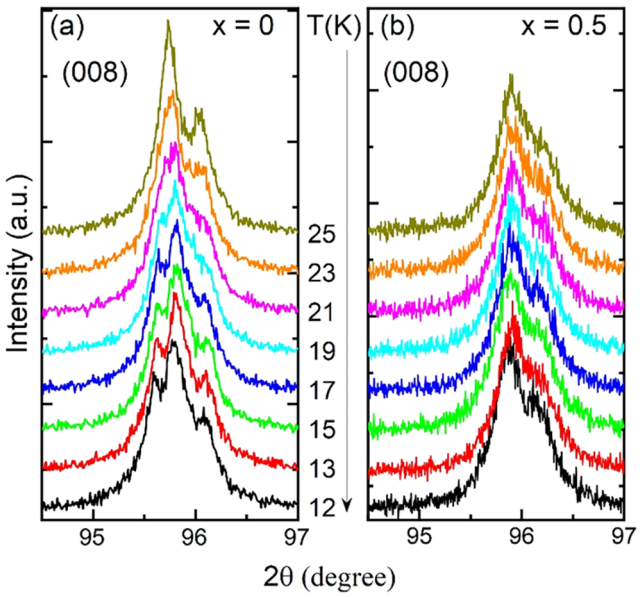


**Figure 7.** Temperature-dependent X-ray diffraction profiles of the (008) reflection for (a) GCO and (b) GMCO, illustrating the evolution of possible lattice distortion with decreasing temperature.

Figure 8a,b shows the Rietveld refined XRD patterns of GCO and GMCO, collected at 12 K. The insets in each figure enlarged the view of the (0 0 8) peak. The XRD pattern of GCO can be very well refined using tetragonal symmetry $I4_1/amd$ within the available resolution limit, whereas the pattern of GMCO has been refined using cubic symmetry, similar to the RT pattern. The refined lattice parameters at 12 K for GCO are 5.8777(1) and $c$ = 8.3004(1) Å, whereas for GMCO the lattice parameter is 8.29658(9) Å. The refined structural parameters for GCO at 12 K are listed in Table 1.

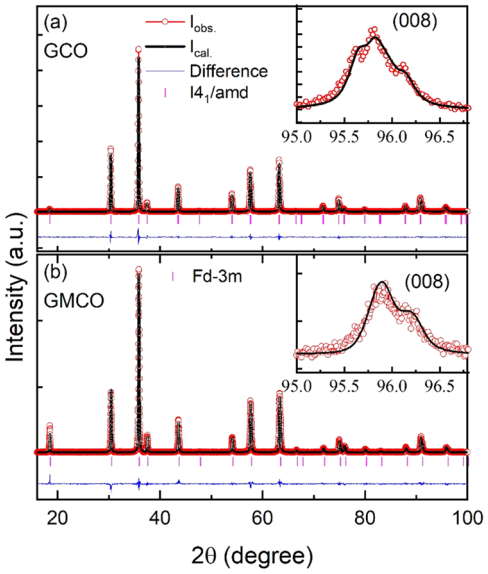


**Figure 8.** Rietveld refined XRD patterns of (a) GCO and (b) GMCO measured at 12 K.

**Table 1. Refined Structural Parameters of GCO at 12 K, obtained from Rietveld Refinement using Tetragonal Symmetry ($I4_1/amd$)[a]**

| atoms (site) | $x$ | $y$ | $z$ | $B$ (Å$^2$) |
|---|---|---|---|---|
| Ge (8$b$) | 0 | 0.25 | 0.375 | 0.92(5) |
| Co (16$c$) | 0 | 0 | 0 | 0.65(5) |
| O (32$e$) | 0 | 0.5010 | 0.2519 | 1.10(1) |

[a]The refined lattice constants are $a$ = 5.8777(1) and $c$ = 8.3004(1) Å. Goodness-of-fit indicators: GoF = 1.61, $R_p$ = 7.13%.

**Neutron Powder Diffraction.** Figure 9a presents the NPD patterns collected at selected temperatures and measured with $\lambda$ = 2.41 Å. The difference curves are also depicted in Figure 9b for the selected temperatures. While cooling the sample below $T_c$, the intensities of some of the nuclear reflections such as (111) and (220) at lower $2\theta$ increase significantly, indicating a commensurate FiM order in


https://doi.org/10.1021/acs.chemmater.5c01331
Chem. Mater. 2025, 37, 5995−6003

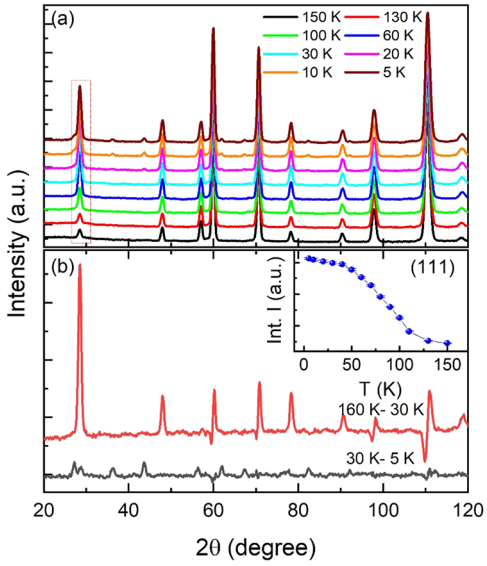


**Figure 9.** Neutron powder diffraction patterns of $Ge_{1-x}Mn_xCo_2O_4$ recorded at selected temperatures. (a) Temperature-dependent diffraction patterns highlighting the emergence of magnetic Bragg peaks at low temperatures. (b) Difference patterns obtained by subtracting the high-temperature data, revealing two distinct sets of magnetic reflections associated with different magnetic sublattices or phases. The inset in panel (b) shows the temperature evolution of the (111) magnetic peak intensity.

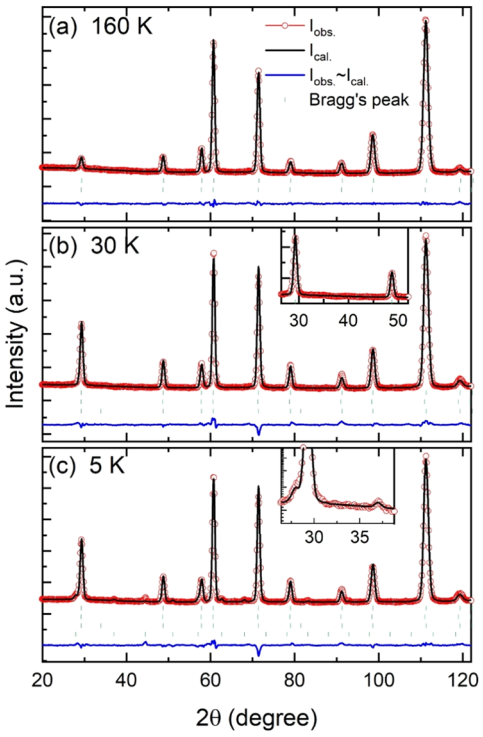


**Figure 10.** Neutron powder diffraction patterns of $Ge_{1-x}Mn_xCo_2O_4$ measured at (a) 160 K (above the magnetic ordering), (b) 30 K, and (c) 5 K. In panel (a) two sets of nuclear Bragg peaks from the primary and secondary crystalline phases are visible. Panels (b, c) each show nuclear (upper) and magnetic (lower) reflections. Inset in panel (b) (around $2\theta$ = 34°) confirms the absence of the (200) peak, confirming the absence of an additional AFM component in $Mn_{0.74}Ge_{0.18}Co_2O_4$. The inset in panel (c) highlights the low-angle magnetic reflections associated with Co ordering in $Ge_{0.91}Mn_{0.18}Co_2O_4$.

$Mn_{0.74}Ge_{0.18}Co_2O_4$, associated with the propagation vector (0,0,0). The integrated intensity of the (111) reflection highlighted within the box region is plotted in the inset of Figure 9b. As the temperature decreases below $T_N$, several new peaks emerge adjacent to nuclear reflections, originating from the AFM ordering of Co spins in $Ge_{0.91}Mn_{0.19}Co_2O_4$. These additional magnetic reflections, clearly visible in the difference data (30−5 K) given in Figure 9b, are associated with the propagation vector (1/2, 1/2, 1/2), analogous to the parent compound GCO.[21,26,29]

Figure 10 shows the refined NPD patterns in the paramagnetic state at 160 K (above $T_c$) and in the magnetic ordered state below $T_N$, at 30 and 5 K. The 160 K data was used as a paramagnetic reference to estimate the scale factor. The 160 K data was refined using two nuclear phases, $Mn_{0.74}Ge_{0.18}Co_2O_4$ and $Ge_{0.91}Mn_{0.18}Co_2O_4$. The relative phase fractions of these two phases were kept fixed, as obtained from the refinement of the RT Echidna data, given in Figure 5. At 30 K, the strongest magnetic intensity is observed at the (111) reflection, confirming a FiM order with propagation vector (0,0,0). We did not observe any intensity at the location of the (200) reflection; see the inset of Figure 10b. This suggests complete absence of any additional AFM component, unlike $Ti_{1-x}Mn_xCo_2O_4$, where a weak intensity of (200) reflection is evident.[30] To solve the magnetic structure of the Mn-rich main phase, irreducible representations (IRREP) were calculated using the BASIREPS program with Mn at (1/8,1/8,1/8) and Co at the (1/2,1/2,1/2) site. Out of the 10 possible IRREPs, the data could be fitted well only with Γ8 of dimension 3 contained only 1 time in Γ8. During the refinement, the occupancies and scale factor were kept fixed, identical to those of the 160 K refinement. The AFM coupled moments at the A and B sites exhibit collinear ferrimagnetic ordering, where the moments are aligned along the [001] and [00−1] directions. Furthermore, the absence of the magnetic (2 0 0) cubic peak excludes the Yafet−Kittel (Y−K)-type spin-canted structure and supports the collinear magnetic structures. The $R_{wp}$ and $\chi^2$ values at 30 K are 7.48 and 6.15, respectively. The resultant magnetic structure of $Mn_{0.74}Ge_{0.18}Co_2O_4$ is shown in Figure 11a, whereas the temperature variation of the A-site ($Mn_A$) and B-site ($Co_B$) moments are shown in Figure 11b. As the sample is cooled, both the $Mn_A$ and $Co_B$ moment sizes increase and attain the maximum value of around 20 K, which remains almost constant upon further cooling to 5 K. At 30 K, the Mn moment is 2.30(4) $\mu_B$ and the Co moment is 1.79(3) $\mu_B$, which is consistent with the values of A- and B-site moments in similar systems.[29,30]

For the magnetic structure refinement below 25 K associated with AFM ordering of Co spins in $Ge_{0.91}Mn_{0.18}Co_2O_4$, an additional magnetic phase with the propagation vector (1/2, 1/2, 1/2) was added in the input file (.pcr) to account for the extra magnetic peaks appearing below 22 K. The resultant magnetic structure in this minor phase resembles the parent compound GCO.[12,18] Also, for the refinement of the magnetic structure in this secondary phase, the scale factor is kept the same as that of the second nuclear phase $Ge_{0.91}Mn_{0.18}Co_2O_4$. The average B-site moment at 5 K in this secondary phase is 2.53(5) $\mu_B$, which is consistent with the parent compound.[30] At 5 K, the average A and B site moments in the main phase are 2.31(3) and 1.82(3) $\mu_B$. The inset in Figure 11b exhibits the temperature dependence of the refined Co moment in the


https://doi.org/10.1021/acs.chemmater.5c01331
Chem. Mater. 2025, 37, 5995−6003

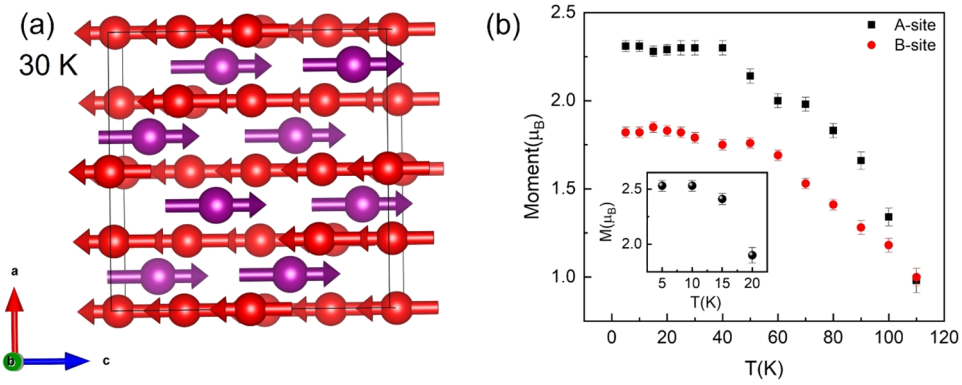


**Figure 11.** (a) Refined magnetic structure at 30 K, with A-site and B-site magnetic ions shown as red and violet spheres and arrows, respectively. (b) Temperature dependence of the average magnetic moments on A-site (red) and B-site (violet) sublattices. The inset in panel (b) shows the temperature evolution of the Co moment in the secondary phase.

minor Ge-rich phase. The Mn atoms in this Ge-rich phase do not participate in the magnetic ordering below 22 K.

## CONCLUSIONS

A comprehensive study of the crystal and magnetic structures of $Ge_{1-x}Mn_xCo_2O_4$ has been conducted, revealing the effects of Mn substitution on magnetostructural properties. The findings were compared with those of $GeCo_2O_4$ to understand the influence of the added disorder at the A site. SEM-EDX analyses in GMCO reveal nanoscale compositional inhomogeneities, providing crucial insights into phase separation and local stoichiometry that are not captured by bulk techniques. The GMCO sample predominantly consists of two distinct spinel phases, differentiated by A-site occupancy: a Mn-rich primary phase $Mn_{0.74}Ge_{0.18}Co_2O_4$ and a minor Ge-rich secondary phase $Ge_{0.91}Mn_{0.19}Co_2O_4$ as confirmed by the EDX analysis and the two-phase Rietveld refinement of the room-temperature neutron powder diffraction data with a phase fraction of approximately 6.3(4)%. Both phases in GMCO adopt a cubic spinel structure with subtle differences in lattice parameters, with values of 8.29642(7) Å for the Mn-rich phase and 8.30751(8) Å for the Ge-rich phase. Comparison of low-temperature structural properties of GCO and GMCO exhibits striking differences, despite having nearly identical structures at room temperature. The low-temperature XRD results confirm a cubic-to-tetragonal transition in GCO associated with magnetic order, which remains absent in GMCO. This may be attributed to the increased disorder at the A site in GMCO, which possibly suppresses the structural distortions linked with magnetic transitions. Similar effects have been observed for other Mn-substituted compounds.[24,30] Ferrimagnetic ordering of Mn and Co spins is confirmed in $Mn_{0.74}Ge_{0.18}Co_2O_4$ below 108 K, while $Ge_{0.91}Mn_{0.18}Co_2O_4$ exhibits AFM ordering of Co spins below 22 K. The refined magnetic moment values in both phases of GMCO are consistent with the reported literature values. Our extensive analyses using SEM-BEX, EDX, X-ray, and neutron diffraction reveal nanoscale compositional inhomogeneities, providing crucial insights into phase separation and local stoichiometry, which are essential for understanding the intrinsic magnetic response of these compounds.

## AUTHOR INFORMATION


### Corresponding Author

**Shivani Sharma** − *National High Magnetic Field Laboratory, Tallahassee, Florida 32310, United States;* orcid.org/0000-0002-3866-6006; Email: phy.shivanisharma@gmail.com

### Authors

**Pooja Jain** − *UGC-DAE Consortium for Scientific Research, Indore 452001, India*

**Benny Schundelmier** − *National High Magnetic Field Laboratory, Tallahassee, Florida 32310, United States;* orcid.org/0000-0002-7345-9977

**Chin-Wei Wang** − *National Synchrotron Radiation Research Center, Hsinchu 300092, Taiwan*

**Poonam Yadav** − *Center for Integrated Nanostructure Physics, Institute for Basic Science, Suwon 16419, Republic of Korea*

**Adrienn Maria Szucs** − *National High Magnetic Field Laboratory, Tallahassee, Florida 32310, United States*

**Kaya Wei** − *National High Magnetic Field Laboratory, Tallahassee, Florida 32310, United States*

**Niranjan P. Lalla** − *UGC-DAE Consortium for Scientific Research, Indore 452001, India*

**Theo Siegrist** − *National High Magnetic Field Laboratory, Tallahassee, Florida 32310, United States; Department of Chemical and Biomedical Engineering, FAMU-FSU College of Engineering, Florida State University, Tallahassee, Florida 32310, United States;* orcid.org/0000-0001-5368-1442

Complete contact information is available at: https://pubs.acs.org/10.1021/acs.chemmater.5c01331


### Notes

The authors declare no competing financial interest.

## ACKNOWLEDGMENTS

A portion of this work was performed at the National High Magnetic Field Laboratory, which is supported by the National Science Foundation Cooperative Agreement No. DMR-2128556 and the State of Florida. B.S. and K.W. acknowledge the support of the NHMFL User Collaboration Grant Program. SEM-BEX and EDX work was performed at the Center for Rare Earths, Critical Minerals, and Industrial Byproducts at the National High Magnetic Field Laboratory, Florida State University, supported by the State of Florida through Contract #0000071627. T.S. acknowledges funding



https://doi.org/10.1021/acs.chemmater.5c01331
Chem. Mater. 2025, 37, 5995−6003

from the National Science Foundation under Grant No. DMR-2219906.

## REFERENCES


(1) Li, Y.; Kan, X.; Liu, X.; Feng, S.; Lv, Q.; Rehman, K. M. U.; Wang, W.; Liu, C.; Wang, X.; Xu, Y. Spin-Glass Evolution Behavior in Spinel Compounds Co2-XZnxSnO4 ($0 \leq x \leq 1$). *J. Alloys Compd.* **2021**, *852*, No. 156962.

(2) Tomiyasu, K.; Ueda, H.; Matsuda, M.; Yokoyama, M.; Iwasa, K.; Yamada, K. Molecular spin-liquid state in the spin-32frustrated spinel HgCr2O4. *Phys. Rev. B* **2011**, *84* (3), No. 035115.

(3) Hoshi, T.; Katori, H. A.; Kosaka, M.; Takagi, H. Magnetic Properties of Single Crystal of Cobalt Spinel. *J. Magn. Magn. Mater.* **2007**, *310*, 2006−2008.

(4) Lashley, J. C.; Stevens, R.; Crawford, M. K.; Boerio-Goates, J.; Woodfield, B. F.; Qiu, Y.; Lynn, J. W.; Goddard, P. A.; Fisher, R. A. Specific Heat and Magnetic Susceptibility of the Spinels GeNi2 O4 and GeCo2 O4. *Phys. Rev. B* **2008**, *78* (10), No. 104406, DOI: 10.1103/PhysRevB.78.104406.

(5) Champion, J. D. M.; Harris, M. J.; Holdsworth, P. C. W.; Wills, A. S.; Balakrishnan, G.; Bramwell, S. T.; Čižmár, E.; Fennell, T.; Gardner, J. S.; Lago, J.; McMorrow, D. F.; Orendáč, M.; Orendáčová, A.; Paul, D. M.; Smith, R. I.; Telling, M. T. F.; Wildes, A. Er2Ti2O7: Evidence of Quantum Order by Disorder in a Frustrated Antiferromagnet. *Phys. Rev. B* **2003**, *68* (2), No. 020401.

(6) Watanabe, T.; Hara, S.; Ikeda, S.-I. Jahn-Teller Inactivity and Magnetic Frustration in GeCo2O4 Probed by Ultrasound Velocity Measurements. *Phys. Rev. B* **2008**, *78* (9), No. 094420.

(7) Anderson, P. W. Ordering and Antiferromagnetism in Ferrites. *Phys. Rev.* **1956**, *102* (4), No. 1008.

(8) Matsuda, T.; Agata, R.; Watanabe, T.; Umeyama, N.; Hara, S.; Tokumoto, M.; Hata, Y.; Yasuoka, H.; Ikeda, S.-I. Frustration Effects in the Spinel Oxide Ge(Fe1−xCox)2O4. *J. Phys.: Conf. Ser.* **2012**, *391* (1), No. 012098.

(9) Balents, L. Spin Liquids in Frustrated Magnets. *Nature* **2010**, *464* (7286), 199−208.

(10) Yadav, P.; Sharma, S.; Sau, T.; da Silva, I.; Lalla, N. P. Jahn-Teller and Geometric Frustration Effects on the Structural and Magnetic Ground States of Substituted Spinels (Ni,A)Cr2O4 (A = Mn/Cu). *J. Alloys Compd.* **2020**, *826*, No. 154139.

(11) Stevens, R.; Woodfield, B. F.; Boerio-Goates, J.; Crawford, M. K. Heat Capacities, Third-Law Entropies and Thermodynamic Functions of the Geometrically Frustrated Antiferromagnetic Spinels GeCo2O4 and GeNi2O4 from T = (0 to 400) K. *J. Chem. Thermodyn.* **2004**, *36* (5), 359−375.

(12) Pramanik, P.; Ghosh, S.; Yanda, P.; Joshi, D. C.; Pittala, S.; Sundaresan, A.; Mishra, P. K.; Thota, S.; Seehra, M. S. Magnetic Ground State, Field-Induced Transitions, Electronic Structure, and Optical Band Gap of the Frustrated Antiferromagnet GeCo 2 O 4. *Phys. Rev. B* **2019**, *99*, No. 134422.

(13) Diaz, S.; De Brion, S.; Chouteau, G.; Canals, B.; Simonet, V.; Strobel, P. Magnetic Frustration in the Spinel Compounds Ge Co2 O4 and Ge Ni2 O4. *Phys. Rev. B* **2006**, *74* (9), No. 092404.

(14) Savary, L.; Balents, L. Quantum Spin Liquids: A Review. *Rep. Prog. Phys.* **2017**, *80* (1), No. 016502.

(15) Fabrèges, X.; Ressouche, E.; Duc, F.; De Brion, S.; Amara, M.; Detlefs, C.; Paolasini, L.; Suard, E.; Regnault, L. P.; Canals, B.; Strobel, P.; Simonet, V. Field-Driven Magnetostructural Transitions in GeCo2 O4. *Phys. Rev. B* **2017**, *95* (1), No. 014428.

(16) Pramanik, P.; Singh, S.; Chowdhury, M. R.; Ghosh, S.; Sathe, V.; Rabe, K. M.; Vanderbilt, D.; Seehra, M. S.; Thota, S. Lattice Dynamics and Magnetic Exchange Interactions in: A Spinel with Pyrochlore Lattice. *Phys. Rev. B* **2021**, *104* (1), No. 014433.

(17) Thota, S.; Reehuis, M.; Maljuk, A.; Hoser, A.; Hoffmann, J. U.; Weise, B.; Waske, A.; Krautz, M.; Joshi, D. C.; Nayak, S.; Ghosh, S.; Suresh, P.; Dasari, K.; Wurmehl, S.; Prokhnenko, O.; Büchner, B. Neutron Diffraction Study of the Inverse Spinels Co2TiO4 and Co2SnO4. *Phys. Rev. B* **2017**, *96* (14), No. 144104.

(18) Diaz, S.; de Brion, S.; Chouteau, G.; Canals, B.; Simonet, V.; Strobel, P. Magnetic frustration in the spinel compounds GeCo2O4and GeNi2O4. *Phys. Rev. B* **2017**, *90* (1), No. 092404.

(19) Barton, P. T.; Kemei, M. C.; Gaultois, M. W.; Moffitt, S. L.; Darago, L. E.; Seshadri, R.; Suchomel, M. R.; Melot, B. C. Structural Distortion below the Néel Temperature in Spinel ${\mathrm{GeCo}}_{2}{\mathrm{O}}_{4}$. *Phys. Rev. B* **2014**, *90* (6), No. 064105.

(20) Lashley, J. C.; Stevens, R.; Crawford, M. K.; Boerio-Goates, J.; Woodfield, B. F.; Qiu, Y.; Lynn, J. W.; Goddard, P. A.; Fisher, R. A. Specific Heat and Magnetic Susceptibility of the Spinels ${\text{GeNi}}_{2}{\text{O}}_{4}$ and ${\text{GeCo}}_{2}{\text{O}}_{4}$. *Phys. Rev. B* **2008**, *78* (10), No. 104406.

(21) Diaz, S.; de Brion, S.; Holzapfel, M.; Chouteau, G.; Strobel, P. Study of Competitive Magnetic Interactions in the Spinel Compounds GeNi2O4, GeCo2O4. *Phys. B: Condens. Matter* **2004**, *346−347*, 146−149.

(22) Diaz, S.; de Brion, S.; Chouteau, G.; Canals, B.; Simonet, V.; Strobel, P. Magnetic Frustration in the Spinel Compounds GeCo2O4and GeNi2O4. *Phys. Rev. B* **2006**, *74* (9), No. 092404.

(23) Matsuda, T.; Agata, R.; Watanabe, T.; Umeyama, N.; Hara, S.; Tokumoto, M.; Hata, Y.; Yasuoka, H.; Ikeda, S.-I. Frustration effects in the spinel oxide Ge(Fe1−xCox)2O4. *J. Phys.: Conf. Ser.* **2012**, *391* (1), No. 012098.

(24) Joy, P. A.; Date, S. K. Unusual Magnetic Hysteresis Behavior of Oxide Spinel MnCo2O4. *J. Magn. Magn. Mater.* **2000**, *210* (1), 31−34.

(25) Mandrus, D.; Keppens, V.; Chakoumakos, B. C.; Granroth, G. E.; Nagler, S. E. A Neutron Diffraction Study of Co2Ru1−xMnxO4 Spinels. *MRS Proc.* **1998**, *547* (1), 177−182.

(26) Matsuda, M.; Hoshi, T.; Katori, H. A.; Kosaka, M.; Takagi, H. Magnetic-Field-Induced Transitions in Spinel GeCo 2 O 4. *J. Phys. Soc. Jpn.* **2011**, *80* (3), No. 034708.

(27) Granroth, G. E.; Mandrus, D.; Keppens, V.; Nagler, S. E. Long- and Short-Range Magnetic Order in the Spinel Co2Ru1−xMnxO4. *J. Magn. Magn. Mater.* **2004**, *272−276*, 1306−1307.

(28) Kaushik, S. D.; Rajeevan, N. E.; Kumar, R. Exploring the Effect of Bi Doping in Cubic Spinel BixCo2-XMnO4 by Employing Neutron Diffraction. *Phys. B: Condens. Matter* **2018**, *551*, 46−50.

(29) Pramanik, P.; Reehuis, M.; Tovar, M.; Hoser, A.; Hoffmann, J. U.; Chen, Y. S.; Lin, J. G.; Weise, B.; Waske, A.; Thota, S. Strong Correlation between Structure and Magnetic Ordering in Tetragonally Distorted Off-Stoichiometric Spinels Mn1.15Co1.85 O4 and Mn1.17Co1.60Cu0.23 O4. *Phys. Rev. Mater.* **2022**, *6* (3), No. 034407.

(30) Pramanik, P.; Joshi, D. C.; Reehuis, M.; Hoser, A.; Hoffmann, J. U.; Manna, R. S.; Sarkar, T.; Thota, S. Neutron Diffraction Evidence for Local Spin Canting, Weak Jahn-Teller Distortion, and Magnetic Compensation in Ti1-XMnxCo2O4 Spinel. *J. Phys.: Condens. Matter* **2020**, *32* (24), No. 245801.

(31) Singha, A. D.; Pramanik, P.; Joshi, D. C.; Ghosh, S.; Jena, S. K.; Tiwari, P.; Sarkar, T.; Thota, S. Reentrant Canonical Spin-Glass Dynamics and Tunable Field-Induced Transitions in (GeMn)Co2O4 Kagomé Lattice. *J. Phys.: Condens. Matter* **2024**, *36* (7), No. 075802.

(32) Rodríguez-Carvajal, J. Recent Advances in Magnetic Structure Determination by Neutron Powder Diffraction. *Phys. B: Condens. Matter* **1993**, *192* (1), 55−69.

(33) Hubsch, J.; Gavoille, G. First Order Magnetic Phase Transition in GeCo2O4. *J. Magn. Magn. Mater.* **1987**, *66* (1), 17−22.

(34) Gopal, E. S. R. *Specific Heats at Low Temperatures*; Springer: Plenum, New York, 1966; Vol. *26*.

(35) Jauch, W.; Reehuis, M.; Bleif, H. J.; Kubanek, F.; Pattison, P. Crystallographic Symmetry and Magnetic Structure of CoO. *Phys. Rev. B* **2001**, *64* (5), No. 052102.

(36) Ding, Y.; Ren, Y.; Chow, P.; Zhang, J.; Vogel, S. C.; Winkler, B.; Xu, J.; Zhao, Y.; Mao, H. Pressure-Induced Long-Range Magnetic Ordering in Cobalt Oxide. *Phys. Rev. B* **2006**, *74* (14), No. 144101.

(37) Jauch, W.; Reehuis, M. Electron Density Distribution in Paramagnetic and Antiferromagnetic CoO: A \ensuremath{\gamma}-Ray Diffraction Study. *Phys. Rev. B* **2002**, *65* (12), No. 125111.




https://doi.org/10.1021/acs.chemmater.5c01331
Chem. Mater. 2025, 37, 5995−6003